Multirate Lane-Keeping System With Kinematic Vehicle Model

Chang Mook Kang, *Member, IEEE*, Seung-Hi Lee, *Member, IEEE*, and Chung Choo Chung, *Member, IEEE*

***Abstract*—In this paper, a novel multirate lane-keeping system (LKS) is introduced by using a kinematic-based model considering a look-ahead distance. First, we developed a kinematic lateral motion model for LKS with respect to the road. To increase a system damping of vehicle, the unique look-ahead output measurement matrix was introduced. The decentralized multirate lane-keeping control scheme with a multirate Kalman filter was also applied to resolve the asynchronous and irregular sampling time of multi sensors in autonomous vehicles. We validated the performance of the proposed kinematic-based multirate LKS using the dynamic vehicle solver CarSim, MATLAB/Simulink, and electric power steering hardware-in-the-loop system. Experimental validation was also conducted using a real test vehicle. Both simulation and experimental results showed that the proposed kinematic-based LKS performed lane-keeping capability comparable to that of dynamic-based LKS. In particular, the experimental results showed that the proposed method, compared to a human driver, can also maintain the lane within reasonable specifications. The experimental validation was performed at vehicle speeds of up to 120 km/h.**

***Index Terms*—Autonomous Vehicle, Kinematic model, Lateral Control, Lane-keeping system.**

NOMENCLATURE

${}^{v}\{xyz\}$	vehicle coordinate frame
y	distance from the center of gravity (c.g.) to the center of turn in ${}^{v}\{xyz\}$
y_{des}	distance from the lane center to the center of turn in ${}^{v}\{xyz\}$
$e_y = y - y_{des}$	lateral lane center offset at c.g.
$e_{yL} = y_L - y_{des,L}$	lateral lane center offset at the look-ahead point
$\psi = \psi_L$	yaw angle
ψ_{des}	yaw angle slope of the lane center
$e_\psi = \psi_{des} - \psi$	heading angle error at c.g.
$\dot{\psi}$	yaw rate
l	distance of the tire from c.g. of the vehicle
u	input ($=\delta$: steer angle)
Subscripts	
f	front
r	rear
v	vision
m	motion
des	desired

Manuscript received October 14, 2017; revised April 21, 2018; accepted July 20, 2018. Date of publication August 8, 2018; date of current version October 15, 2018. This work was supported in part by the Industrial Source Technology Development Program "Automatic lane change system for novice drivers" (10044620) funded by the Ministry of Trade, Industry and Energy (MOTIE, Korea) and in part by the Development of Source Technologies for IT Software Convergence Business (R7117-16-0164—Development of wide area driving environment awareness and cooperative driving technology which are based on V2X wireless communication) funded by the Ministry of Science, ICT and Future Planning, South Korea. The review of this paper was coordinated by Prof. J. Wang. *(Corresponding author: Chung Choo Chung.)*

C. M. Kang was with the Department of Electrical Engineering, Hanyang University, Seoul 04763, South Korea. He is now with the Agency for Defense Development, Daejeon 305-152, South Korea (e-mail: kcm0728@gmail.com).

S.-H. Lee is with the Department of Electrical Engineering, Hanyang University, Seoul 04763, South Korea (e-mail: shlee@ieee.org).

C. C. Chung is with the Division of Electrical and Biomedical Engineering, Hanyang University, Seoul 04763, South Korea (e-mail: cchung@hanyang.ac.kr).

Color versions of one or more of the figures in this paper are available online at http://ieeexplore.ieee.org.

Digital Object Identifier 10.1109/TVT.2018.2864329

I. INTRODUCTION

LATERAL vehicle motion control methods, including lane-keeping systems (LKSs) and lane change systems (LCSs), have been widely studied to enhance vehicle safety and provide riding comfort. Dynamic and kinematic-based methods have been widely developed and used to control the lateral motion of vehicles [1], [2]. However, the dynamic-based control method is generally used than the kinematic-based method because the former can more accurately reflect the dynamic movement of a vehicle than the latter [3]–[7]. To understand and analyze the accurate lateral motion of a vehicle, the dynamic-based method requires several unknown or uncertain parameters such as inertia, tire-road friction, and cornering stiffness. Because of the nonlinear characteristic of these unknown and varying parameters the design of a nonlinear observer is therefore necessary. However, this approach of utilizing a nonlinear observer leads to a high computational complexity. Thus, the dynamic-based method is not necessarily more suitable for developing a low-cost commercial algorithm with embedded electronic control units. Nevertheless, several methods based on the dynamic model (LCSs or LKSs) have been successfully developed and reported [3]–[5], [8]–[10], some of which consider and design a look-ahead distance to improve performance.

In contrast with the dynamic model-based method, the kinematic model-based method does not require unknown vehicle parameters. In other words, the performance of the controller based on kinematics is not influenced by these unknown and varying parameters of a vehicle [1], [2], [11]–[13]. Nevertheless, the kinematic-based model does not effectively reflect the vehicle's motion under aggressive maneuvering situations because the tire slip angle is not negligible under these situations [2], [11]. Therefore, the use of the model was limited to

low-speed situations, such as autonomous parking assistant systems [1], [2], [13]. However, quantitative analyses of the kinematic model-based controller in high-speed or highway driving have seldom been reported.

Although the quantitative analysis of the tire slip angle has been infrequently reported, several studies have reported that this tire slip angle is sufficiently small to approximate in the slalom test at speeds faster than 60 km/h [14], curved road test [15], and other tests [16]–[18]. Furthermore, it was found that the vehicle side slip angle is less than 1° in the highway autonomous or maneuver driving under clothoid constraints [19], [20]. Thus, it is considered that the tire slip angle is also negligible under highway driving conditions, including cases employing an advanced driver assistant system (ADAS). In other words, it is expected that kinematic model-based LKS is sufficient to maintain the lane in highway autonomous driving.

In this study, a novel multirate lane-keeping system using the kinematic-based model considering the look-ahead output measurement matrix is proposed. First, we uniquely modeled the lane-keeping system using the kinematic lateral motion. As previously mentioned, it is observed that the slip angle is sufficiently small to approximate in the ADAS application [14]–[20]. Under this situation, it is expected that the kinematic-based model could sufficiently represent the movement of the vehicle [21]–[24]. Second, we proposed a look-ahead output measurement matrix considering a clothoid constraint to improve the lane-keeping performance. In a previous research, we validated dynamic-based LKS with a look-ahead distance for highway driving [10]. However, the system loses its controllability when a state variable related to a look-ahead distance is chosen in the kinematic-based motion model [22]. We hypothesized that the kinematic-based controller could conduct lane-keeping as efficiently as the dynamic-based controller without the loss of controllability if the proper output measurement matrix was selected [22]. Finally, the multirate LKS scheme was introduced using the multirate Kalman filter (KF) to overcome the asynchronous and irregular sampling time of multi sensors in autonomous vehicles. The multirate KF rapidly estimated the vehicle state associated with an in-vehicle sensor, whereas the camera vision sensor measured the state at a slow rate. The performance of the proposed method was validated using MATLAB/Simulink, dynamic vehicle solver CarSim, and electric power steering system with Micro Autobox from dSPACE Inc. Moreover, experiments were conducted utilizing a sports utility vehicle. Simulation and experimental results confirmed that the kinematic model-based LKS demonstrated reasonable lane-keeping performance as well the dynamic model-based LKS did. Moreover, experimental results showed that the proposed method can maintain the lane within reasonable specifications compared to a human driver. In particular, the proposed LKS, considering a look-ahead output measurement matrix scheme, outperforms the LKS controller at the center of gravity. The contributions of this study are as follows:

- A kinematic lateral motion model of vehicles for a lane-keeping system with respect to the road was developed.
- An output measurement matrix that considers a look-ahead distance was introduced to mimic human behavior.
- A multirate method was applied to compensate for the asynchronous sampling time between the vision sensor and in-vehicle motion sensor. It is possible to control the vehicle according to the ECU sampling time even when the vision information is obtained at a slow rate.

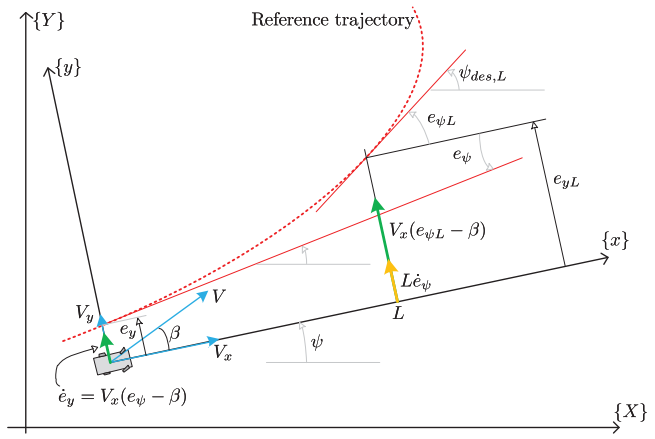

Fig. 1. Lateral motion with look-ahead distance.

II. Vehicle Kinematic Model for a Lane Keeping System

In this section, a vehicle kinematic model for a lane-keeping system is described. The vehicle kinematic motion model was derived with respect to the road lane. The advantages of this model are that it does not require or is influenced by unknown vehicle parameters [2]. From Fig. 1 the development of a unique vehicle kinematic model for the lane-keeping system using the state vector $\mathbf{x}(k) = \left[\, e_y(k)\ e_\psi(k)\ \dot{\psi}(k) \,\right]$. Note that the lateral acceleration of the vehicle in highway driving is small because of road design conditions [19], [20]. Therefore, it is assumed that the lateral velocity is constant or slowly varying. This assumption also applies to the process of deriving the dynamic lateral motion model [2]. The vehicle kinematic model can be developed using the following derivation procedures [19], [20], [22].

From $e_y = y - y_{des}$, $\dot{e}_y$ is derived as follows [2]

$$\begin{aligned} \dot{e}_y &= \dot{y} - \dot{y}_{des} \\ &= V_y + V_x e_\psi \\ &= \frac{l_r}{l_f + l_r} V_x \tan\delta + V_x e_\psi \\ &\approx \frac{l_r}{l_f + l_r} V_x \delta + V_x e_\psi . \end{aligned} \tag{1}$$

From the bicycle model, the kinematics of yaw motion is derived with the assumptions that V_x is constant or slowly varying, and δ is small. With these assumptions, the vehicle's yaw

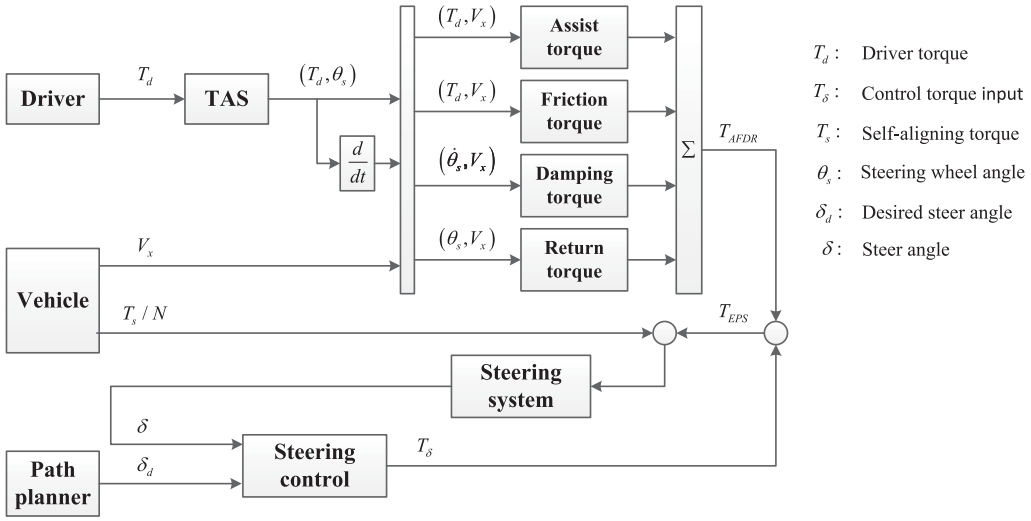

Fig. 2. Lateral control structure of autonomous vehicle. Here, N denotes the gear ratio of EPS. T_{AFDR} denotes the total sum of assist, friction, damping and return torque. The path planner includes the ADASs such as LKS and LCS, and gives the desired steer angle to the steering control system.

motion can be approximated as

$$\dot{\psi} = \frac{V}{l_f + l_r}\sin(\delta) = \frac{V_x}{l_f + l_r}\tan(\delta) \approx \frac{V_x}{l_f + l_r}\delta$$
$$\ddot{\psi} = \frac{V_x}{l_f + l_r}\dot{\delta}. \tag{2}$$

Next, the following third-order discrete-time state-space model is derived using the state vector $\mathbf{x}(k) = \left[e_y(k)\ e_\psi(k)\ \dot{\psi}(k)\right]$, control input $u(k) = \delta(k)$, and external signals $\varphi(k) = \left[\dot{\psi}_{des}(k)\ \delta(k-1)\right]^T$

$$e_y(k+1) = e_y(k) + \frac{l_r}{l_f + l_r}V_x T\delta(k) + V_x T e_\psi(k)$$
$$e_\psi(k+1) = e_\psi(k) + T\dot{\psi}_{des}(k) - T\dot{\psi}(k)$$
$$\dot{\psi}(k+1) = \dot{\psi}(k) + \frac{V_x}{l_f + l_r}\delta(k) - \frac{V_x}{l_f + l_r}\delta(k-1) \tag{3}$$
$$\mathbf{x}(k+1) = \Phi\mathbf{x}(k) + \Gamma u(k) + \Gamma_\varphi\varphi(k) \tag{4}$$

where

$$\Phi = \begin{bmatrix} 1 & TV_x & 0 \\ 0 & 1 & -T \\ 0 & 0 & 1 \end{bmatrix},\ \Gamma = \begin{bmatrix} \frac{l_r}{l_f + l_r}V_x T \\ 0 \\ \frac{V_x}{l_f + l_r} \end{bmatrix}$$
$$and\ \Gamma_\varphi = \begin{bmatrix} 0 & 0 \\ T & 0 \\ 0 & -\frac{V_x}{l_f + l_r} \end{bmatrix}. \tag{5}$$

Here, the sampling time T is given by the electronic control unit (ECU).

Indeed, the electric power steering system (EPS) model corresponding to the low-level part of the vehicle should be included when designing a lateral motion controller, as shown in Fig. 2. The EPS torque consists of the assist, friction, damping, and return torques. The EPS torque was designed to improve vehicle handling characteristics, and it typically has nonlinear characteristics. However, we designed the upper-level lane-keeping controller using the kinematic lateral motion model assuming that a lower-level EPS controller is capable of tracking the desired steer angle at high speeds, and response characteristics of the lower-level controller are not extremely fast in the ADAS application.

III. Decentralized Multirate State Estimation

The sampling rate of the vision sensor is slower than that of the in-vehicle motion sensor. Thus, the output of the controller remains constant during the sample period of the vision sensor. In other words, the vehicle receives a control input with a slower sample time synchronized with the slower sensor (e.g., vision sensor). Moreover, the update rates of several sensors used in vehicle applications are different from one another [10]. Therefore, we made use of the multirate state estimation scheme to provide control at a fixed sample time.

The update rate of the motion sensor, T_m, is typically the same as the ECU update rate, T, in a commercial in-vehicle network ($T_m = T$). However, the update rate of the vision sensor is either irregular or asynchronous. Thus, one can decompose the state-space representation given by Eq. (4) into two subsystems based on each sensor: $\mathbf{x}(k) = \left[\mathbf{x_v}(\mathbf{k})^{\mathbf{T}}\ \mathbf{x}_m(k)^T\right]$. $\mathbf{x}_v(k) = \left[e_y(k)\ e_\psi(k)\right]$ is associated with a vision sensor and $\mathbf{x}_m(k) = \left[\dot{\psi}(k)\right]$ is associated with a motion sensor. Note that the output matrix is $C = \mathrm{diag}(C_v, C_m)$, where $C_v = \mathrm{diag}(1,1)$ and $C_m = [1]$, and the output vector is $\mathbf{y}(k) = \left[\mathbf{y_v}(\mathbf{k})^{\mathbf{T}}\ \mathbf{y}_m(k)^T\right]$ where $\mathbf{y}_v(k) = \left[e_y(k)\ e_\psi(k)\right]$ and $\mathbf{y}_m(k) = \left[\dot{\psi}(k)\right]$.

Assumption 1: The update period of the vision sensor, T_v, is an integer multiple of the sampling period of ECU for lateral

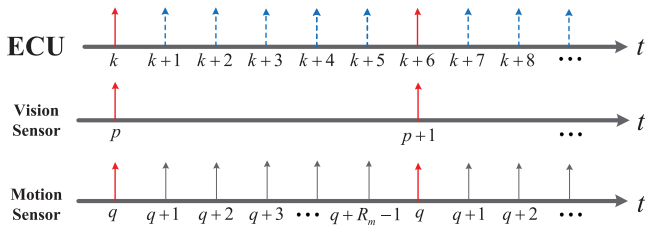

Fig. 3. Multirate update scheme for asynchronous sensors. Here, $T_v = 6\,T$.

motion control, such as

$$T_v = R_m T,$$

where $R_m \in \mathbb{N}$ and $R_m \geq 1$. ◊

With **Assumption 1**, a time instant, t, can be represented as

$$t = \left(p + \frac{q}{R_m}\right) T_v \tag{6}$$

for $p = 0, 1, \ldots$ and $q = 0, 1, \ldots, R_m - 1$. Here, p and q denote the update instant of vision processing and update instant of control, respectively. In the interim, the ECU is operating at a rate of $1/T$, as shown in Fig. 3.

The prediction states $\bar{\mathbf{x}}_m(k), \bar{\mathbf{x}}_v(k)$ and correction states $\hat{\mathbf{x}}_m(k), \hat{\mathbf{x}}_v(k)$ are described as follows:

• Motion sensor (fast)

$$\begin{aligned}\bar{\mathbf{x}}_m(p, q+1) &= \Phi_m \hat{\mathbf{x}}_m(p, q) + \Gamma_m u(p, q) \\ &\quad + \Phi_{mv} \hat{\mathbf{x}}_v(p, q) + \Gamma_{m\varphi} \varphi(p, q) \\ \hat{\mathbf{x}}_m(p, q) &= \bar{\mathbf{x}}_m(p, q) + L_m \left(\mathbf{y}_m(p, q) - C_m \bar{\mathbf{x}}_m(p, q)\right)\end{aligned} \tag{7}$$

where

$$\Phi_m = [1],\ \Phi_{mv} = \begin{bmatrix}0\\0\end{bmatrix}^T,\ \Gamma_m = \left[\frac{V_x}{l_f + l_r}\right],\ \Gamma_{m\varphi} = \begin{bmatrix}0\\ -\frac{V_x}{l_f + l_r}\end{bmatrix}^T.$$

At this point, a multirate decentralized state estimator is developed for each sensor. These utilize multirate multi sensor data to estimate the state from the vision sensor. To estimate the state, x_v, we made use of a multirate state estimation [25]:

• Vision sensor (slow)

$$\begin{aligned}\bar{\mathbf{x}}_v(p, q+1) &= \Phi_v \hat{\mathbf{x}}_v(p, q) + \Gamma_v u(p, q) \\ &\quad + \Phi_{vm} \hat{\mathbf{x}}_m(p, q) + \Gamma_{v\varphi} \dot{\psi}_{des}(p, q) \\ \hat{\mathbf{x}}_v(p, q) &= \bar{\mathbf{x}}_v(p, q) + L_v \left(\mathbf{y}_v(p, 0) - C_v \bar{\mathbf{x}}_v(p, 0)\right)\end{aligned} \tag{8}$$

where

$$\Phi_v = \begin{bmatrix}1 & TV_x\\ 0 & 1\end{bmatrix},\ \Phi_{vm} = \begin{bmatrix}0\\ -T\end{bmatrix},\ \Gamma_v = \begin{bmatrix}\frac{l_r}{l_f + l_r} V_x T\\ 0\end{bmatrix}$$

$$\text{and } \Gamma_{v\varphi} = \begin{bmatrix}0 & 0\\ T & 0\end{bmatrix}.$$

Here, L_m and L_v are estimator gains to be determined.

Definition 1: A multirate state estimator is considered convergent if it is convergent at some sampling periods. ◊

Assuming that the output measurement, $\mathbf{y}_v(\cdot)$ is available at each sampling instant, pT_v, we aim for the multirate state estimator, (7), to converge at the sampling period T_v.

Remark 1: Consider a simple case with the assumption that $R_m = T_v/T$ is fixed. Applying discrete-time lifting leads to the following lifted model:

$$\begin{aligned}\bar{\mathbf{x}}_v(p+1, 0) &= \left(\Phi_v^{Rm} - \sum_{n=1}^{R_{m\,v}} \Phi_v^n L_v C_v\right) \bar{\mathbf{x}}_v(p, 0) \\ &\quad + \sum_{n=1}^{R_{m\,v}} \Phi_v^n \mathbf{y}_v(p, 0).\end{aligned} \tag{9}$$

Here, we define $\Phi_v^{R_{m\,v}} \tilde{L}_v = (\sum_{n=1}^{R_{m\,v}} \Phi_v^n) L_v$ and choose the estimator gain to stabilize $\Phi_v^{Rm} - \Phi_v^{Rm} \tilde{L}_v C_v$. Then, we immediately can compute

$$L_v = \left(\sum_{n=1}^{R_{m\,v}} \Phi_v^n\right)^{-1} \Phi_v^{R_{m\,v}} \tilde{L}_v. \tag{10}$$

This estimator gain guarantees the convergence of the state estimator, (7), at the instant of each fixed-period vision sensor update. ◊

Theorem 1: The decentralized multirate state estimators given in Eqs. (7) and (8) are robustly convergent for $R_m \in Z_{R_m}$ with gains of L_m for the Schur stability of Eq. (7) and L_v for the robust Schur stability of Eq. (8) from Eq. (10). ◊

Proof: Without loss of generality, assume $u(\cdot) = 0$ and zero external signals for the convergence analysis. Moreover, assume that time indices $q + R_m$ and $p + 1$ are synchronous for $R_m \in \mathbb{Z}_{R_m}$. Accordingly, we have $R_m T = T_v$ [26]. ■

IV. Controller Design

It is well known that considering a look-ahead distance can improve the lateral control performance by increasing the damping effect on a vehicle [8], [27]–[31]. Thus, the objective of designing a controller is to steer the vehicle using a look-ahead distance as would a human driver. However, the equation of the kinematic-based vehicle model, Eq. (4) does not include the look-ahead distance. Therefore, we designed a look-ahead output measurement matrix considering a clothoid constraint.

A. Look-ahead Output Measurement Matrix

In this section, the clothoid constraint is introduced. A clothoid curve is used for a vehicle to transition smoothly from one curvature value to another. The curvature of the clothoid curve at arc lengths s is described as follows:

$$\kappa = 6c_3 s + 2c_2 \tag{11}$$

where $2c_2$ is the road curvature at $s = 0$, and $6c_3$ is the rate of road curvature. By integrating Eq. (11), the clothoid cubic polynomial curve road model can be obtained as follows [19],

[20]:

$$f_c(s) = c_0 + c_1 s + c_2 s^2 + c_3 s^3 \tag{12}$$

where $c_0 = e_y$ denotes the lateral lane center offset at $s = 0$, and $c_1 = e_\psi$ denotes the heading angle error at $s = 0$. The arc length s can be approximated by the look-down range distance x at a small curvature.

From Eq. (12), the lateral offset at the look-ahead distance is defined as follows:

$$e_{yL} = f_c(L). \tag{13}$$

In fact, c_3 is sufficiently small to be neglected in autonomous highway driving $\|c_3\| \leq 10^{-6} m^{-1}$ [10]. To consider e_{yL} rather than e_y, which is defined as the state vector, the first state variable is reformulated using the above clothoid constraints. Letting the first state variable, $y_1(\cdot)$, denote the lateral offset at a look-ahead distance, L, leads to

$$\begin{aligned} y_1(k) &= e_{yL}(k) \\ &= c_0 + c_1 L + c_2 L^2 + c_3 L^3 \\ &\approx e_y(k) + e_\psi(k) L + \frac{\dot{\psi}(k)}{2V_x} L^2. \end{aligned} \tag{14}$$

Next, the output measurements matrix using Eq (14) were designed to incorporate the look-ahead distance of the vehicle into the controller. The relationship between the output vector $\mathbf{y}(k)$ and state vector $\mathbf{x}(k) = \left[e_y(k)\ e_\psi(k)\ \dot{\psi}(k) \right]$ is as follows:

$$\mathbf{y}(k) = C\mathbf{x}(k)$$

where

$$C = \begin{bmatrix} 1 & L & \dfrac{L^2}{2V_x} \\ 0 & 1 & 0 \\ 0 & 0 & 1 \end{bmatrix}. \tag{15}$$

Notice that we may choose the measurement matrix as a diagonal matrix, $C_o = I_{3\times 3}$, because all states are measurable. The parameters e_y and e_ψ are obtained from the camera and $\dot{\psi}$ is measured from the inertia sensor. However, the nominal measurement matrix, C_o, can not consider the look-ahead distance of the vehicle, i.e., the vehicle is only controlled at the c.g. and this approach may cause yaw rate oscillation [8], [27]–[31].

B. Optimal Look-ahead Output Feedback Controller

The optimal output feedback controller is then designed to consider the look-ahead distance of the vehicle. Thus, the kinematic-based LKS was designed using our output measurement matrix, (15). The following output feedback control is used for LKS:

$$u(k) = -K_y \mathrm{y}(k) \tag{16}$$

where K_y is the optimal output feedback gain. This optimal gain can be obtained by solving the discrete-time algebraic Riccati equation (DARE) to minimize the following linear quadratic cost function

$$J = \sum_{k=0}^{N} (\mathrm{y}(k)^T Q_y \mathrm{y}(k) + u(k)^T R_u u(k)) \tag{17}$$

where Q_y and R_u are symmetric weighting matrices. The output cost term $\mathrm{y}(k)^T Q_y \mathrm{y}(k)$ is transformed into the state cost $\mathrm{x}(k)^T Q_x \mathrm{x}(k)$ with $Q_x = C^T Q_y C$.

When designing a controller using a typical output feedback, the range of the control input is less than of the state feedback controller. However, for the proposed output measurement matrix, a transformation matrix, H, satisfying homoeomorphism always exists between C_o and C, as follows:

$$C = HC_o. \tag{18}$$

Therefore, an optimal output feedback controller equivalent to the optimal state feedback can be designed at any time because of homoeomorphism. In other words, there always exists a weighting matrix of the output cost, Q_y, equivalent to the weighting matrix of the state cost, Q_x, as follows:

$$\begin{aligned} \mathrm{y}(k)^T Q_y \mathrm{y}(k) &= \mathrm{x}(k)^T C^T Q_y C \mathrm{x}(k) \\ &= \mathrm{x}(k)^T C_o^T H^T Q_y H C_o \mathrm{x}(k) \\ &= \mathrm{x}(k)^T Q_x \mathrm{x}(k). \end{aligned} \tag{19}$$

The proposed output feedback method can move the pole of the closed-loop more freely than a typical output feedback controller. At this stage, the optimal output feedback gain can be obtained from K_x as follows by solving DARE:

$$K_y = -\left(R_u + \Gamma^T P \Gamma\right)^{-1} \Gamma^T P \Phi C^{-1}, \tag{20}$$

where $P > 0$ is the maximal solution to the following DARE. Here, system matrices Φ and Γ are given by Eq. (5).

$$P = \Phi^T P \Phi - (\Phi^T P \Gamma)(R_u + \Gamma^T P \Gamma)^{-1} (\Gamma^T P \Phi) + Q_x. \tag{21}$$

Consequently, the state feedback controller is defined as follows:

$$\begin{aligned} u(k) &= -K_y \mathrm{y}(k) \\ &= -K_y C \mathrm{x}(k). \end{aligned} \tag{22}$$

Accordingly, the vehicle is controlled at a look-ahead distance using $e_{yL}(k)$. Moreover, the controller can consider a look-ahead distance using the optimal feedback gain, K_y, from DARE and optimize the lateral offset error at a look-ahead distance. This look-ahead output matrix approach can guide the direction by selecting the weighting matrix, Q_y, which regulates the lateral offset error at the look-ahead distance. Note that, without an estimator, the proposed optimal look-ahead output feedback controller will synchronously operate with slower periodic sensors. However, the proposed multirate decentralized estimator allows the proposed controller to operate synchronously with the ECU sample time.

V. Application Results

The proposed method was validated via computational simulation results with CarSim from Mechanical Simulation, MATLAB/Simulink from MathWorks, and an EPS system equipped

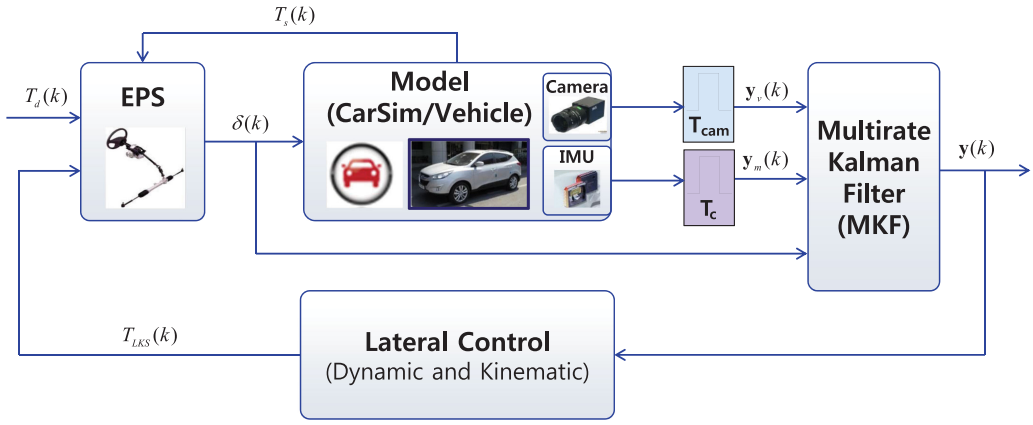

Fig. 4. Block diagram of the lane keeping system with an electric power steering system.

TABLE I
VEHICLE PARAMETERS

Vehicle parameter	Symbol	Value	Unit
Total mass	m	1,515	kg
Distance from c.g. to the front axle	l_f	0.967	m
Distance from c.g. to the rear axle	l_r	1.673	m
Yaw moment of inertia	I_z	3,392	kgm^2
Front tire cornering stiffness	$C_{\alpha f}$	118,800	N/rad
Rear tire cornering stiffness	$C_{\alpha r}$	165,300	N/rad

with Autobox from dSPACE. Experiments using a test vehicle were also conducted. The structure of the proposed lane keeping system is described in Fig. 4. Using this lane keeping system, the performance of the proposed kinematic-based LKS was compared to the dynamic-based LKS in simulations and experiments, respectively.

We used the following dynamic model for the comparison [10], [20]: the state vector $\mathbf{x}_d = [e_{yL}\ \dot{e}_y\ e_\psi\ \dot{\psi}]^T$, the control input $u = \delta$ and external signals $\varphi_d = [\dot{\psi}_{des}\ e_{\psi L} - e_\psi\ ]^T$. The definitions of these parameters are listed in Table I.

$$\begin{aligned}\dot{\mathbf{x}}_d &= A\mathbf{x}_d + Bu + B_\varphi \varphi_d \\ &= \begin{bmatrix} A_v & A_{vm} \\ A_{mv} & A_m \end{bmatrix} \mathbf{x}_d + \begin{bmatrix} B_v \\ B_m \end{bmatrix} u + \begin{bmatrix} B_{v\varphi} \\ 0 \end{bmatrix} \varphi_d. \end{aligned} \tag{23}$$

where

$$A_v = \begin{bmatrix} 0 & 1 & 0 \\ 0 & a_{22} & a_{23} \\ 0 & 0 & 0 \end{bmatrix},\ A_m = \begin{bmatrix} a_{44} \end{bmatrix},\ A_{vm} = \begin{bmatrix} -L \\ a'_{24} \\ -1 \end{bmatrix},$$

$$A_{mv} = \begin{bmatrix} 0 \\ a'_{42} \\ a_{43} \end{bmatrix}^T,\ B_v = \begin{bmatrix} 0 \\ b'_{21} \\ 0 \end{bmatrix},\ B_m = \begin{bmatrix} b_{41} \end{bmatrix},\ B_{v\varphi} = \begin{bmatrix} L & V_x \\ V_x & 0 \\ 1 & 0 \end{bmatrix}$$

with

$$a_{22} = -\frac{2(C_{\alpha f} + C_{\alpha r})}{mV_x},\ \ a_{23} = -a_{22}V_x,$$

$$a_{24} = -1 - \frac{2(C_{\alpha f} l_f - C_{\alpha r} l_r)}{mV_x^2},\ \ a'_{24} = (a_{24} - 1)V_x,$$

$$a_{42} = -\frac{2(C_{\alpha f} l_f - C_{\alpha r} l_r)}{I_z},\ \ a'_{42} = \frac{a_{42}}{V_x},$$

$$a_{43} = -a_{42},\ a_{44} = -\frac{2(C_{\alpha f} l_f^2 + C_{\alpha r} l_r^2)}{I_z V_x},$$

$$b_{21} = \frac{2C_{\alpha f}}{mV_x},\ \ b'_{21} = b_{21}V_x,\ \ b_{41} = \frac{2C_{\alpha f} l_f}{I_z}.$$

A. Simulations

The EPS hardware-in-the-loop-simulation (HILS) system was used for simulations, and the overall system structure is shown in Fig. 5. The EPS HILS system is composed of the EPS system and Autobox from dSPACE. Springs were mounted to emulate the simplified self-aligning torque of the vehicle [32]. The torque angle sensor (TAS) was used to measure the torque and steering wheel angle. All signals were logged through a controller network area interface. MicroAutBox DS1501 from dSPACE Inc. was used as an embedded real-time controller with a sampling time of 10 ms. The nominal values of EPS parameters were used but are not described in this paper because they contain proprietary information. AutoBox DS1005 from dSPACE Inc. was used for an embedded real-time dynamic solver, CarSim.

The lower-level backstepping controller for tracking the desired steering wheel angle described in [32] was applied in both kinematic and dynamic-based LKSs. In upper-level LKS, using the dynamic lateral model, unknown vehicle parameters were replaced by nominal constant values of a C-class vehicle in CarSim, as listed in Table I. The same values for other available parameters, such as the length of the vehicle, were used in both kinematic and dynamic-based models. The longitudinal speed of the vehicle used in both dynamic and kinematic models was constant, i.e., 110 *km/h*. The vehicle traveled a third-order cubic polynomial S curved road, satisfying clothoid constraints. In the

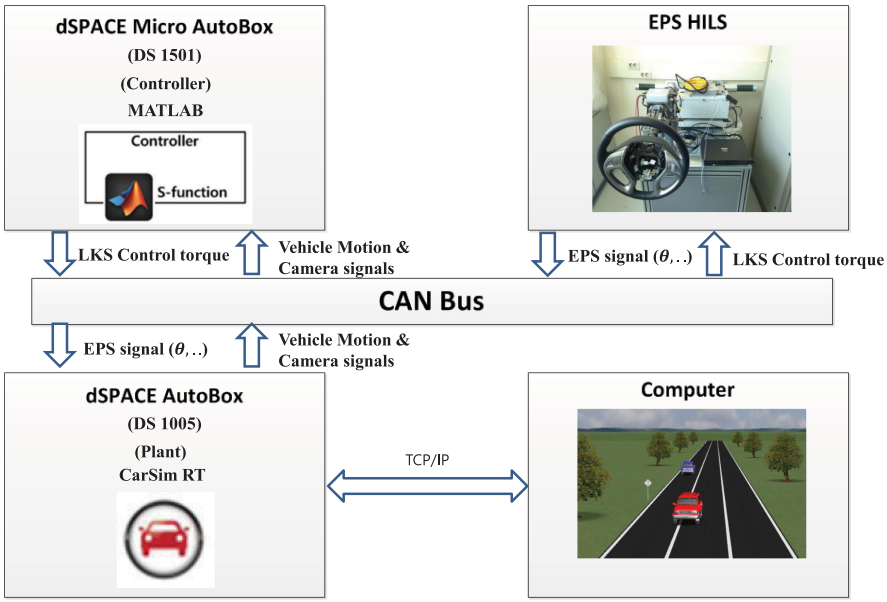

Fig. 5. Overall structure of the lane keeping system with electric power steering systems, dSPACE AutoBox and CarSim.

simulation, the lane information was obtained every 60 *ms* from the camera sensor. The sample time of LKS and motion sensor was 10 *ms*. Although it is more efficient to vary the look-ahead distance with respect to the driving condition, constant values were used for the validation of model characteristics.

Measured steering wheel angle and torque signals from TAS according to both kinematic and dynamic models at 110 *km/h* are described in Fig. 6. Furthermore, the vehicle response with respect to the road (e_y) is described in Fig. 6(c). Considering that the main objective of LKS is to drive the vehicle in the lane center, unknown and nonlinear parameters such as inertia and cornering stiffness were dynamically changed during simulations. Although we simulated the proposed algorithm with an EPS HILS, including nonlinear characteristics, the proposed kinematic-based method exhibited a lane-keeping performance that was as good as that of the dynamic-based method. The magnitudes of both kinematic and dynamic LKS input torques for lane-keeping are similar to hardware-in-the-loop simulations. It can be observed that of the proposed kinematic-based LKS demonstrates reasonable performance in the lateral offset compared to that of the dynamic-based LKS at high-speeds, as shown in Fig. 6(c).

In Fig. 7, the system damping effect of the vehicle can be observed, depending on the look-ahead output measurement matrix. The green line shows lane-keeping control performance without a look-ahead distance, whereas the red dashed line shows the performance considering the look-ahead distance. As expected, without the look-ahead output measurement matrix in the LKS, the vehicle followed a path with oscillations in both the steering wheel angle and torque. The lateral offset, which is one of the key component in LKS, was also considerably oscillated without the look-ahead output measurement matrix, as shown in Fig. 7(c). Controlling the vehicle without using the look-ahead distance means that the system is only looking down and driving. Thus, it is expected that as the speed increases, the higher the oscillation magnitude becomes. However, considering the look-ahead distance, the proposed method (red dashed line) showed no oscillation in its control performance for either torque or steering wheel angle. This confirms that the proposed kinematic-based LKS with the look-ahead output measurement matrix outperforms the LKS without such a matrix.

B. *Experiments with a Test Vehicle*

The vehicle tested was a small sports utility vehicle (Tucson by Hyundai). A camera vision sensor from Mobileye was installed in the test vehicle, as shown in Fig. 8. The camera sensor was mounted at the front window shield. The torque angle sensor was used to measure the driver torque, T_d, and the steering wheel angle, θ_s. On-board sensors such as a yaw rate sensor, and a wheel speed sensor were also used to check the vehicle responses. The yaw rate sensor was mounted at the center of gravity of the vehicle. Moreover, a wheel speed sensor was mounted on each wheel. The sampling time of the vehicle's motion sensor was 10 *ms* whereas that of the camera vision sensor was 70 *ms*. The update period of the vision sensor (Mobileye) is not a constant value because of the image processing. However, lane information was received at fixed intervals through other companies, which cannot be disclosed for security reasons.

The same control algorithm used in the simulation was embedded in MicroAutobox from dSPACE using MATLAB/Simulink. The control sample time of LKS was 10 *ms* because of the multirate control method. The longitudinal speed of the vehicle was set at 30 m/s using adaptive cruise control. Tests, employing a real vehicle, were conducted at the high-speed circuit of Korea Automobile Testing & Research Institute (KATRI) (http://eng.ts2020.kr/), as shown in Fig. 9. The specifications of the high-speed circuit are listed below:

- Total length : 5,040 m

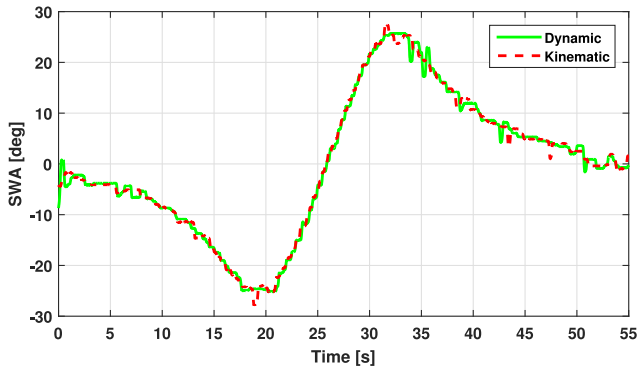

(a)

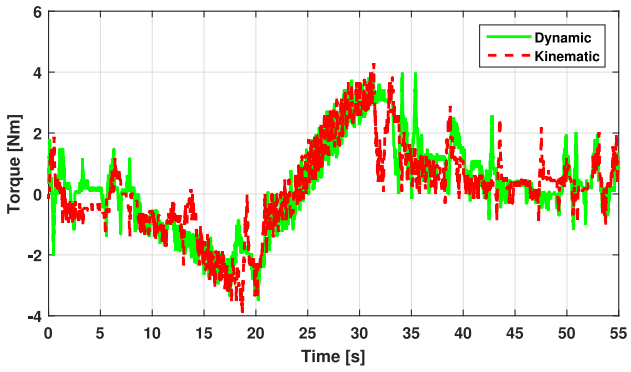

(b)

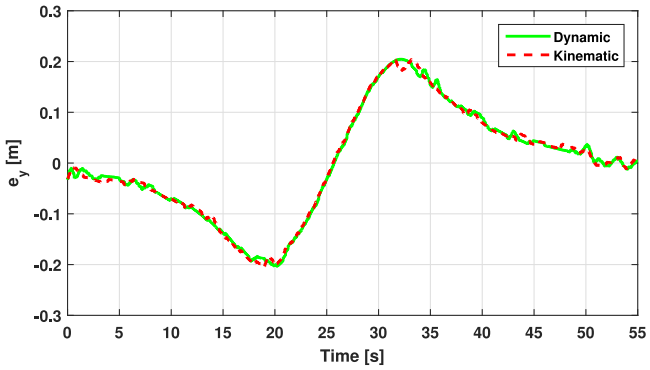

(c)

Fig. 6. Steering wheel angle (SWA), torque and vehicle response (e_y) from each model-based controller at 110 *km/h*. (a) Steering wheel angle. (b) Torque input. (c) Lateral offset.

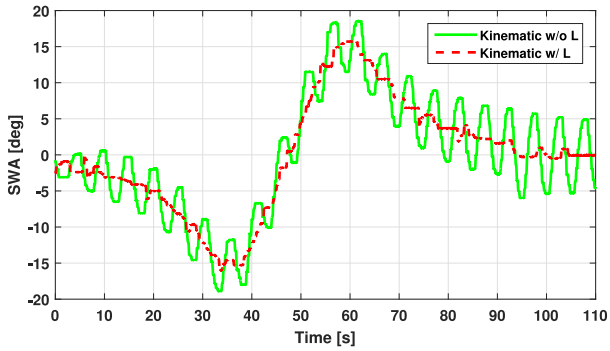

(a)

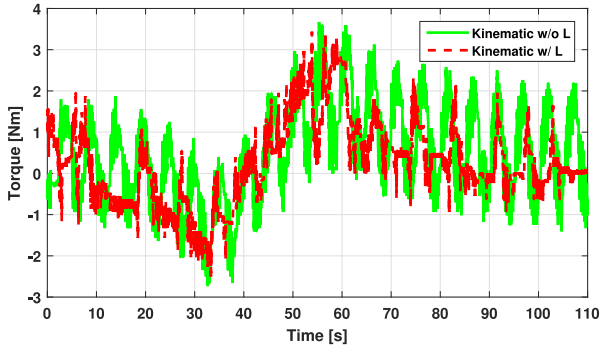

(b)

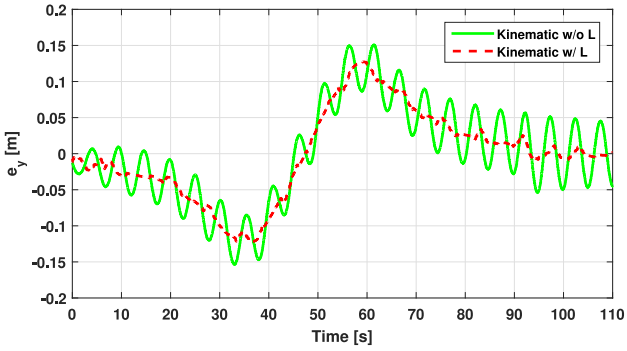

(c)

Fig. 7. Steering wheel angle (SWA), torque and vehicle response (e_y) with the kinematic model-based controller: with look-ahead distance ($L = 20$ m) and without look-ahead distance ($L = 0$), respectively. (a) Steering wheel angle. (b) Torque input. (c) Lateral offset.

- Width : 21.2 to 25.7 m (four-lane)
- Max bank angle : 42°
- Max speed : 250 km/h (designed speed 180 km/h)
- Line configuration
  - Straight line section 967 m × 2,
  - Relief section 411 × 4,
  - Curve line section 731 × 2
- Curve radius : 360 m.

The LKS torque, steering wheel angle, and states for kinematic and dynamic vehicle lateral motion models are shown in Figs. 10 and 11, respectively. In the low-speed experiment, the vehicle performed lane-keeping in a straight road at 60 *km/h*, whereas the vehicle in the high-speed experiment tracked the high speed circuit. The lateral offset at the look-ahead distance e_y, was obtained from the camera vision sensor using Eq. (13). The look-ahead distance used in the experiment was 20 m. Different from the dynamic lateral motion model, the derivative of the lateral offset in the kinematic lateral motion model was not shown because $\dot{e}_y$ was not modeled. It was observed that the input torque and steering wheel angle from the kinematic and dynamic model-based LKSs were similar in the simulation and experiment. Experimental data from

(a)

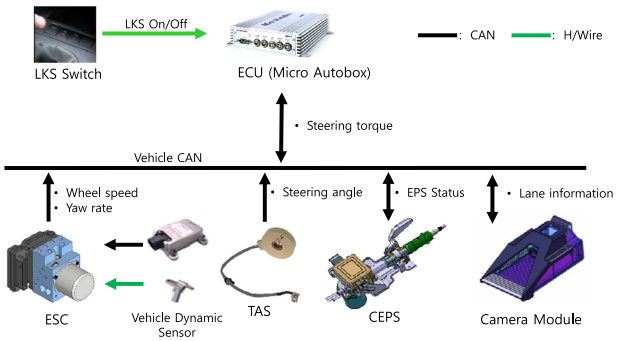

(b)

Fig. 8. Test vehicle [32]. (a) Photo of test vehicle. (b) Block diagram of test vehicle.

Fig. 9. High speed circuit of KATRI.

an expert human driver were also obtained for comparision with lane-keeping characteristics. By observing the yaw rate, $\dot{\psi}$, which shows the motion of the vehicle chassis, it was concluded that both kinematic and dynamic model-based LKSs controlled the vehicle in a manner similar to an expert human driver.

To enable repeated experiments, longitudinal control was performed using the adaptive cruise control. The speeds are shown in Figs. 12(a) and 13(a), whereas lane coefficients from the camera vision sensor are shown in Figs. 12(b) and 13(b). The lane-keeping performance can be evaluated from the lateral lane center offset at the center of gravity, c_0, and the

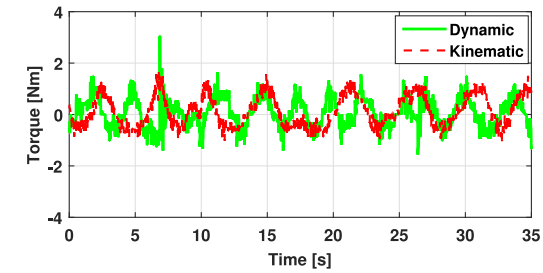

(a)

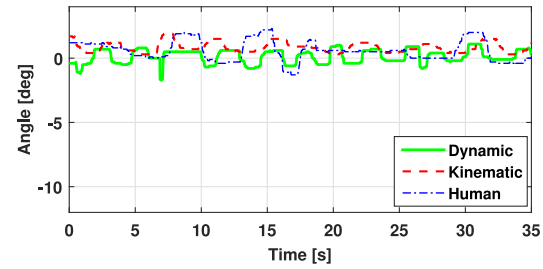

(b)

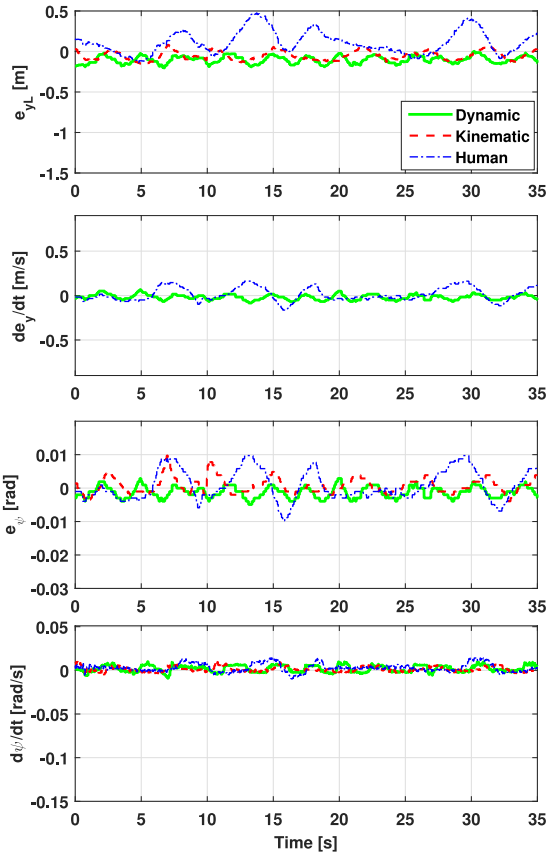

(c)

Fig. 10. LKS torque, steering wheel angle and states at 60 *km/h*. (a) LKS torque. (b) Steering wheel angle. (c) Vehicle states.

heading angle error at the center of gravity, c_1. The expert driver maintained a lane, which is within 0.4 m, whereas the kinematic and the dynamic model-based LKSs showed reasonable performance, which is within 0.2 m in the low-speed experiments. In the high-speed experiments, the lane-keeping

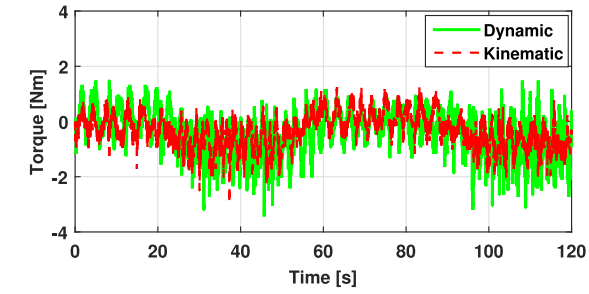

(a)

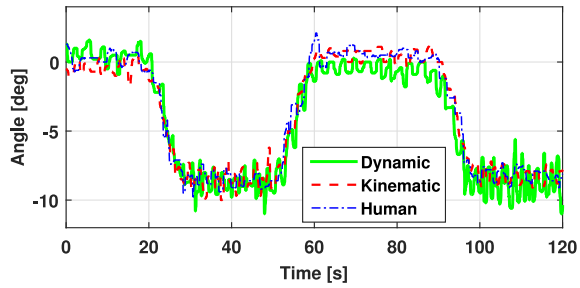

(b)

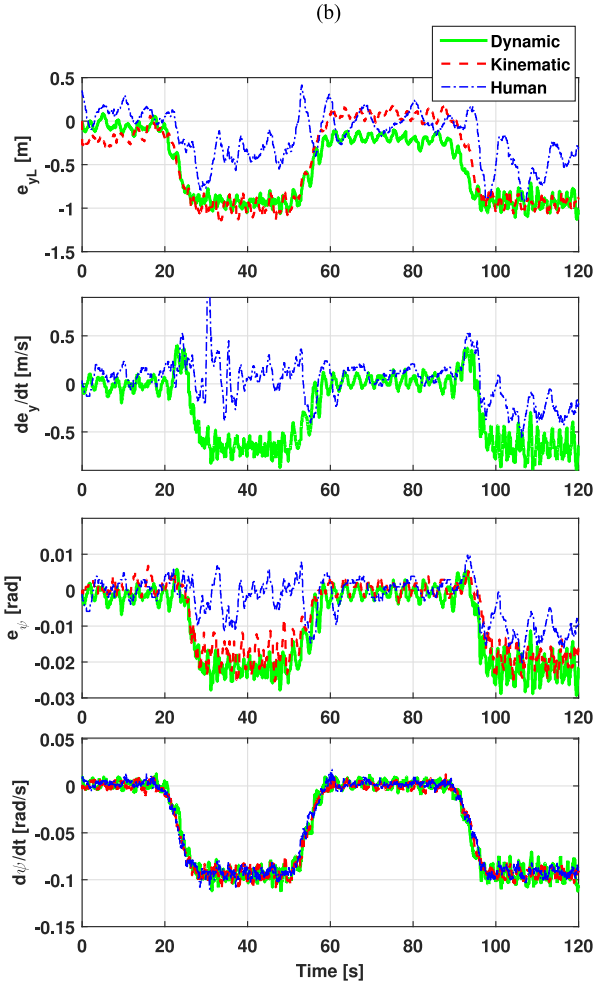

(c)

Fig. 11. LKS torque, steering wheel angle and states at 120 *km/h*. (a) LKS torque. (b) Steering wheel angle. (c) Vehicle states.

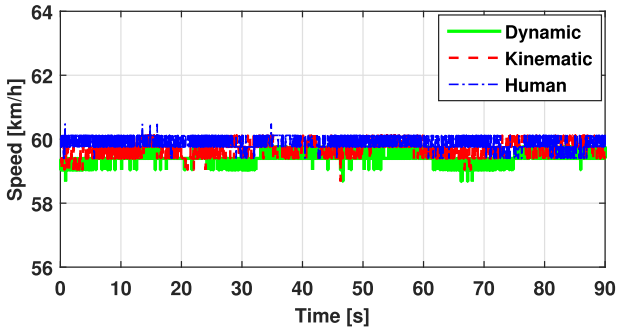

(a)

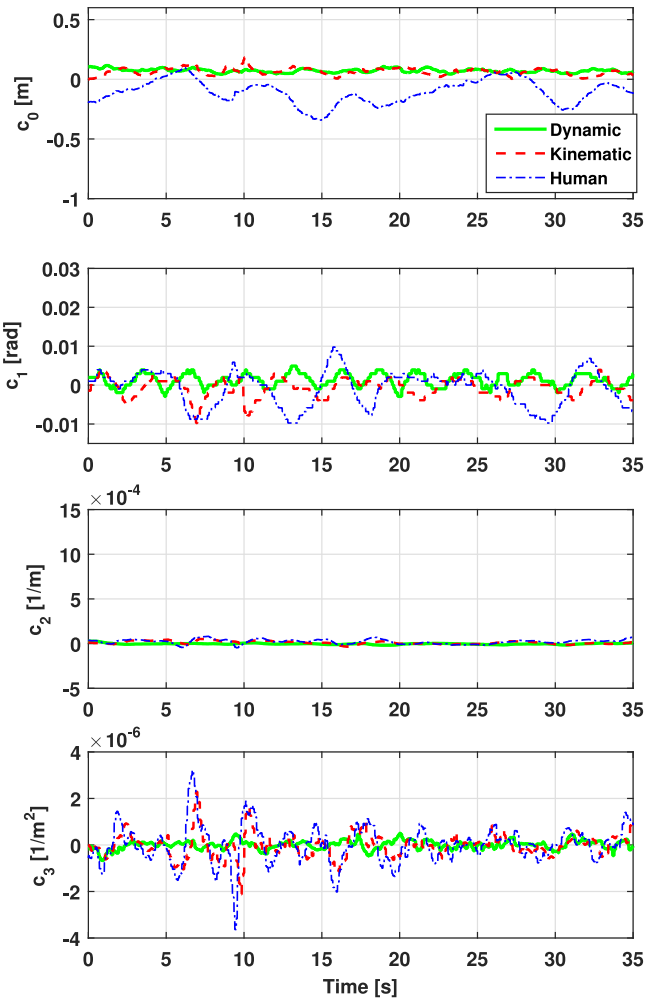

(b)

Fig. 12. Dataset at low speed: 60 *km/h*. (a) Longitudinal speed. (b) Lane coefficients from the camera.

performance of the driver deteriorated, but both controllers maintained lanes that are within reasonable amounts. Overall, the numerical results of experiments for the lateral offset are summarized in Table II. Both kinematic and dynamic methods could maintain the vehicle in the lane center when com-

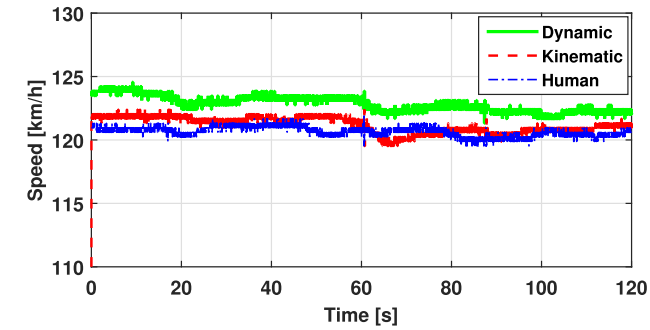

(a)

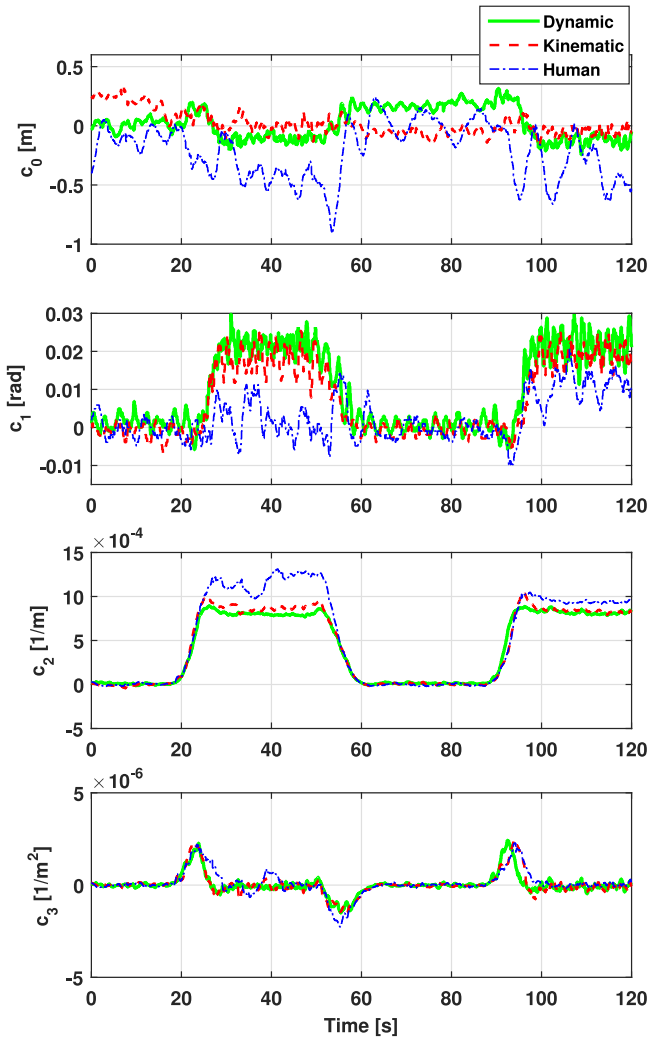

(b)

Fig. 13. Dataset at high speed: 120 *km/h*. (a) Longitudinal speed. (b) Lane coefficients from the camera.

pared to a human driver. However, without consideration of human factors, it cannot be concluded that LKSs outperform the human driverm such as the frequency of yaw rate. Accordingly, we are considering developing an LKSs that considers human factors, which are seen to be critical problems in the near future.

TABLE II
NUMERICAL COMPARISON RESULTS FOR THE LATERAL OFFSET e_y

		Dynamic	Kinematic	Human driver
$60km/h$	Min [m]	0.0410	-0.0020	-0.3418
	Max [m]	0.1152	0.1836	0.0957
	Mean [m]	0.0725	0.0640	-0.1044
	STD [m]	0.0154	0.0294	0.0991
$120km/h$	Min [m]	-0.1602	-0.1719	-0.9082
	Max [m]	0.3203	0.3281	0.3613
	Mean [m]	0.0118	0.01899	-0.1859
	STD [m]	0.08745	0.09944	0.2505

Minimum, maximum, mean and standard deviation (STD) of each method are presented.

VI. CONCLUSION

In this paper, a novel multirate lane-keeping system using the kinematic vehicle motion, considering the look-ahead distance, is proposed. We developed a kinematic lateral motion model with respect to the road for an LKS which does not require unknown vehicle parameters. To increase system damping and mimic a human driver, a look-ahead output measurement matrix considering look-ahead distance was also introduced. This look-ahead output measurement matrix reduced the oscillation in the control performance in both the torque and steering wheel angle. Moreover, the multirate lane keeping control scheme was proposed using the multirate Kalman filter to resolve the asynchronous and irregular sampling time of multi sensors in autonomous vehicles.

To control performance of the model was validated via computational simulation results with CarSim, MATLAB/Simulink, and an electric power steering system. Experimental results obtained from a test vehicle equipped with Autobox from dSPACE showed that the proposed kinematic vehicle-motion-model-based lateral controller performed lane-keeping as well as the dynamic vehicle-lateral-motion-model-based controller. Compared to a human driver, the proposed method can keep the lane within reasonable specifications. In future work, we will validate the proposed algorithm under a more dynamic situation such as collision avoidance.

REFERENCES

[1] U. Kiencke and L. Nielsen, *Automotive Control Systems*, vol. 2. New York, NY, USA: Springer-Verlag, 2005.
[2] R. Rajamani, *Vehicle Dynamics and Control*. New York, NY, USA: Springer-Verlag, 2011.
[3] C. Hatipoglu, U. Ozguner, and K. A. Redmill, "Automated lane change controller design," *IEEE Trans. Intell. Transp. Syst.*, vol. 4, no. 1, pp. 13–22, Mar. 2003.
[4] J. Ackermann, "Robust car steering by yaw rate control," in *Proc. IEEE Conf. Decis. Control*, 1990, pp. 2033–2034.
[5] H. A. Pham and J. Hedrick, "A robust optimal lateral vehicle control strategy," in *Proc. IEEE Int. Conf. Control Appl.*, 1996, pp. 361–366.
[6] Y. Xia, F. Pu, S. Li, and Y. Gao, "Lateral path tracking control of autonomous land vehicle based on ADRC and differential flatness," *IEEE Trans. Ind. Electron.*, vol. 63, no. 5, pp. 3091–3099, May 2016.

[7] L. Li, Y. Lu, R. Wang, and J. Chen, "A three-dimensional dynamics control framework of vehicle lateral stability and rollover prevention via active braking with MPC," *IEEE Trans. Ind. Electron.*, vol. 64, no. 4, pp. 3389–3401, Apr. 2017.
[8] H.-S. Tan, B. Bougler, and W.-B. Zhang, "Automatic steering based on roadway markers: From highway driving to precision docking," *Vehicle Syst. Dyn.*, vol. 37, no. 5, pp. 315–338, 2002.
[9] S.-H. Lee, Y. O. Lee, Y. Son, and C. C. Chung, "Multirate active steering control for autonomous vehicle lateral maneuvering," in *Proc. IEEE Intell. Vehicles Symp.*, 2012, pp. 772–777.
[10] Y. S. Son, W. Kim, S.-H. Lee, and C. C. Chung, "Robust multirate control scheme with predictive virtual lanes for lane-keeping system of autonomous highway driving," *IEEE Trans. Veh. Technol.*, vol. 64, no. 8, pp. 3378–3391, Aug. 2015.
[11] U. Ozguner, T. Acarman, and K. Redmill, *Autonomous Ground Vehicles*. Norwood, MA, USA: Artech House, 2011.
[12] S. A. Arogeti and N. Berman, "Path following of autonomous vehicles in the presence of sliding effects," *IEEE Trans. Veh. Technol.*, vol. 61, no. 4, pp. 1481–1492, May 2012.
[13] R. Rajamani, C. Zhu, and L. Alexander, "Lateral control of a backward driven front-steering vehicle," *Control Eng. Practice*, vol. 11, no. 5, pp. 531–540, 2003.
[14] Y.-H. J. Hsu, S. M. Laws, and J. C. Gerdes, "Estimation of tire slip angle and friction limits using steering torque," *IEEE Trans. Control Syst. Technol.*, vol. 18, no. 4, pp. 896–907, Jul. 2010.
[15] S. Saraf and M. Tomizuka, "Slip angle estimation for vehicles on automated highways," in *Proc. Amer. Control Conf.*, 1997, vol. 3, pp. 1588–1592.
[16] J.-O. Hahn, R. Rajamani, and L. Alexander, "GPS-based real-time identification of tire-road friction coefficient," *IEEE Trans. Control Syst. Technol.*, vol. 10, no. 3, pp. 331–343, May 2002.
[17] D. Piyabongkarn, R. Rajamani, J. A. Grogg, and J. Y. Lew, "Development and experimental evaluation of a slip angle estimator for vehicle stability control," *IEEE Trans. Control Syst. Technol.*, vol. 17, no. 1, pp. 78–88, Jan. 2009.
[18] M. Doumiati, A. Charara, A. Victorino, and D. Lechner, *Vehicle Dynamics Estimation using Kalman Filtering: Experimental Validation*. Hoboken, NJ, USA: Wiley, 2012.
[19] C. M. Kang, S.-H. Lee, and C. C. Chung, "Lane estimation using a vehicle kinematic lateral motion model under clothoidal road constraints," in *Proc. IEEE Int. Conf. Int. Transp. Syst.*, 2014, pp. 1066–1071.
[20] C. M. Kang, S.-H. Lee, and C. C. Chung, "Comparative evaluation of dynamic and kinematic vehicle models," in *Proc. IEEE Conf. Decis. Control*, 2014, pp. 648–653.
[21] J. Kong, M. Pfeiffer, G. Schildbach, and F. Borrelli, "Kinematic and dynamic vehicle models for autonomous driving control design," in *Proc. IEEE Intell. Vehicles Symp.*, 2015, pp. 1094–1099.
[22] C. M. Kang, S.-H. Lee, and C. C. Chung, "A comparative study of lane keeping system: Dynamic and kinematic models with look-ahead distance," in *Proc. IEEE Intell. Vehicles Symp.*, 2015, pp. 1038–1043.
[23] P. Polack, F. Altché, B. D'Andréa-Novel, and A. De La Fortelle, "The kinematic bicycle model: A consistent model for planning feasible trajectories for autonomous vehicles?" in *Proc. IEEE Intell. Vehicles Symp.*, 2017, pp. 812–818.
[24] G. Cesari, G. Schildbach, A. Carvalho, and F. Borrelli, "Scenario model predictive control for lane change assistance and autonomous driving on highways," *IEEE Intell. Transp. Syst. Mag.*, vol. 9, no. 3, pp. 23–35, Fall 2017.
[25] S.-H. Lee, "Multirate digital control system design and its application to computer disk drives," *IEEE Trans. Control Syst. Technol.*, vol. 14, no. 1, pp. 124–133, Jan. 2006.
[26] S.-H. Lee and C. C. Chung, "Robust multirate on-road vehicle localization for autonomous highway driving vehicles," *IEEE Trans. Control Syst. Technol.*, vol. 25, no. 2, pp. 577–589, Mar. 2017.
[27] K.-T. Feng, H.-S. Tan, M. Tomizuka, and W.-B. Zhang, "Look-ahead human-machine interface for assistance of manual vehicle steering," in *Proc. Amer. Control Conf.*, 1999, vol. 2, pp. 1228–1232.
[28] J. Kosecka, R. Blasi, C. Taylor, and J. Malik, "Vision-based lateral control of vehicles," in *Proc. IEEE Int. Conf. Intell. Transp. Syst.*, 1997, pp. 900–905.
[29] C. J. Taylor, J. Košecká, R. Blasi, and J. Malik, "A comparative study of vision-based lateral control strategies for autonomous highway driving," *The Int. J. Robot. Res.*, vol. 18, no. 5, pp. 442–453, 1999.
[30] H. Peng *et al.*, "Preview control for vehicle lateral guidance in highway automation," *J. Dyn. Syst., Meas. Control*, vol. 115, pp. 679–679, 1993.
[31] H. Pham, K. Hedrick, and M. Tomizuka, "Combined lateral and longitudinal control of vehicles for IVHS," in *Proc. Amer. Control Conf.*, 1994, vol. 2, pp. 1205–1206.
[32] W. Kim, Y. S. Son, and C. C. Chung, "Torque-overlay-based robust steering wheel angle control of electrical power steering for a lane-keeping system of automated vehicles," *IEEE Trans. Veh. Technol.*, vol. 65, no. 6, pp. 4379–4392, Jun. 2016.

Chang Mook Kang (S'14–M'18) received the B.S. and Ph.D. degrees in electrical engineering from Hanyang University, Seoul, South Korea, in 2012 and 2018, respectively.

In 2018, he joined Agency for Defense Development, Daejeon, South Korea, as a Senior Research Engineer. His research interests include control theory, autonomous driving, machine learning, and system integration of intelligent vehicles. He is a Member of the IEEE INTELLIGENT TRANSPORTATION SYSTEMS SOCIETY, the IEEE CONTROL SYSTEMS SOCIETY, the SOCIETY OF AUTOMOTIVE ENGINEERS, the KOREAN SOCIETY OF AUTOMOTIVE ENGINEERS, and the INSTITUTE OF CONTROL, ROBOTICS AND SYSTEMS.

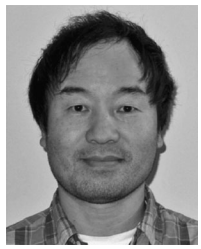

Seung-Hi Lee (M'00) received the B.S. degree in mechanical engineering from Korea University, Seoul, South Korea, the M.S. degree in mechanical engineering from Seoul National University, Seoul, South Korea, in 1985 and 1987, respectively, and the Ph.D. degree in mechanical engineering and applied mechanics from the University of Michigan, Ann Arbor, MI, USA, in 1993.

From 1988 to 1989, he was a Research Scientist with the Korea Institute of Science and Technology. After 1994, he was with the Samsung Advanced Institute of Technology, Suwon, South Korea, where he was a Team Leader responsible for advanced servomechanical systems. In 2009, he joined Hanyang University, Seoul, South Korea, as a Research Professor, where he is also teaching advanced control systems. His research interests include robust sampled-data feedback control of uncertain systems, as well as its application to information storage, automotive, electromechanical, and manufacturing systems. He was a Member of the Editorial Board of the *International Journal of Control, Automation, and Systems*.

Chung Choo Chung (S'91–M'93) received the B.S. and M.S. degrees in electrical engineering from Seoul National University, Seoul, South Korea, and the Ph.D. degree in electrical and computer engineering from the University of Southern California, Los Angeles, CA, USA, in 1993. From 1994 to 1997, he was with the Samsung Advanced Institute of Technology, Suwon, South Korea. In 1997, he joined the Faculty of Hanyang University, Seoul, South Korea.

Dr. Chung was an Associate Editor for the *Asian Journal of Control* from 2000 to 2002 and an (Founding) Editor for the *International Journal of Control, Automation and Systems* from 2003 to 2005. He served as an Associate Editor for various international conferences, such as the IEEE Conference on Decision and Control, the American Control Conferences, the IEEE Intelligent Vehicles Symposium, and the Intelligent Transportation Systems Conference. He was a Guest Editor for a special issue on advanced servo control for emerging data storage systems published by the IEEE TRANSACTIONS ON CONTROL SYSTEM TECHNOLOGIES (TCST), 2012, and also a Guest Editor for the *IEEE Intelligent Transportation Systems Magazine*, 2017. He is currently an Associate Editor for TCST, the IEEE TRANSACTIONS ON INTELLIGENT TRANSPORTATION SYSTEMS, and the *IFAC Mechatronics*. He was a Program Co-chair of ICCAS-SICE 2009, Fukuoka, Japan, an Organizing Chair for the INTERNATIONAL CONFERENCE ON CONTROL, AUTOMATION AND SYSTEMS 2011, KINTEX, South Korea, and a Program Co-chair of the 2015 IEEE INTELLIGENT VEHICLES SYMPOSIUM, COEX, South Korea. He is currently a General Co-chair of CDC 2020, to be held in South Korea. He is also the 2018 President-Elect of the Institute of Control, Robotics and Systems, South Korea.